Available online at www.sciencedirect.com
SCIENCE DIRECT®
Chemical Physics 299 (2004) 225–231
Chemical Physics
www.elsevier.com/locate/chemphys

Ligand effects on the X-ray absorption of a nickel porphyrin complex: a simulation study

Luke Campbell [a,b], Satoshi Tanaka [c], Shaul Mukamel [a,*]

[a] Department of Chemistry, University of California Irvine, Irvine, CA 92697-2025, USA
[b] Advanced Light Source, Lawrence Berkeley National Laboratory, USA
[c] CIAS, Osaka Prefecture University, Sakai 599-8531, Japan

Received 28 July 2003; accepted 1 August 2003

Abstract

We present a simulation of the X-ray absorption near-edge spectrum (XANES) of the metal porphyrin NiTPP (nickel tetraphenylporphyrin) and investigate the changes to the spectrum caused by adding piperidine ligands to the metal atom. The main features in the experimental spectrum (Chen et al., Science 292 (2001) 262) are interpreted in terms of changes in the electronic structure.

1. Introduction

Resonant X-ray spectroscopy provides an excellent local probe for electronic structure. With the advent of ultrafast (attosecond) X-ray sources [1] it is now possible to probe electron motions and chemical processes (e.g., the formation or breaking of chemical bonds) in real time. Time-resolved X-ray diffraction and/or time-resolved X-ray absorption spectroscopy (XAS) are the most appropriate tool to directly determine the molecular structure in the transient stages in chemical reactions without making any assumptions about adiabatic potentials [2,3].

Recently Chen et al. have performed experiments of time-resolved Ni K-edge XAS of NiTPP(Pip)$_2$ (NiTPP, nickel tetraphenylporphyrin; Pip, piperidine) in solution to determine the transient molecular structure following optical-pulse excitation [4]. Since porphyrins have wide applications in many biophysical processes ranging from photosynthesis in chlorophylls to oxygen binding, it is of great interest to clarify the nature of photoinduced structural change of the heme-like porphyrins. The excited state dynamics of NiTPP(Pip)$_2$ have been studied by ultrafast optical pump–probe absorption and Raman spectroscopies [5–8]. In the ground state the divalent Ni ion adopts a triplet spin state $^3(3d_{x^2-y^2}, 3d_{z^2})T^0$. After the transition to the optically excited triplet state T^*, the T^* state immediately decays to the singlet spin state S^* through intersystem crossing, and this is followed by the subsequent dissociation of the apical ligands to yield the S^0 state with square planar geometry (NiTPP). This process proceeds within a few hundred picoseconds [7]. In strongly coordinating solvents, the S^0 state reacts with two piperidine molecules to reform NiTPP(Pip)$_2$ within 28 ns.

There has been an extensive discussion about whether a transient structure, such as a penta-coordinated NiTPP(Pip) structure, is involved along the relaxation from the square-planar S^0 state to the octahedral T^0 ground state. The experiments of Chen et al. did not find such a transient structure. The goals of this study are to provide a method of computing and predicting chemical shifts in X-ray absorption, analyze the experiments by a first-principle simulation of the time-resolved XAS, and examine the conjecture of Chen et al.

2. Theory

Based upon the general formalism developed by Tanaka and Mukamel [9], the optical-pump and X-ray-probe signal intensity is given by

$$W_{\mathrm{PP}} = \sum_l W_{\mathrm{PP}}^l, \tag{1}$$

* Corresponding author. Fax: +949-824-8571.
E-mail address: smukamel@uci.edu (S. Mukamel).

0301-0104/$ - see front matter © 2003 Elsevier B.V. All rights reserved.
doi:10.1016/j.chemphys.2003.08.032

where W_{PP}^{l} stands for the atomic absorption spectrum for the lth site:

$$W_{\mathrm{PP}}^{l} = \frac{1}{2}\frac{1}{\Omega^2\omega}\Re\int \mathrm{d}t \int \mathrm{d}t_3 E_2^*(t)E_2(t-t_3) \times \exp[\mathrm{i}\omega t_3]\mathrm{Tr}\left[\hat{j}_l^{\dagger}(t)\hat{j}_l(t-t_3)\tilde{\rho}^{(2)}(t-t_3)\right], \quad (2)$$

and Ω and ω denotes the central frequencies of optical-pump light and X-ray-probe pulses. Here, $\hat{j}_l(t)$ is the current at site l and the density operator $\tilde{\rho}$ calculated to second order in the pump field is given by Eq. (33) in [9].

For well-separated optical-pump and X-ray-probe pulses, which is the case in the experiment of Chen et al., the four Liouville space pathways shown in Fig. 2 [9] contribute to Eq. (2). In these pathways, $|g\rangle$, $|g'\rangle$ (or $|g''\rangle$), and $|f\rangle$ stand for the ground, optically excited, and X-ray excited states, respectively. Among these pathways, R_1 and R_2 contribute to the signal, while R_3 and R_4 are responsible for the negative (saturated absorption) signal which does not alter the spectral features of XAS itself.

We consider the following adiabatic molecular Hamiltonian, $\hat{H}_{\mathrm{m}}$ [10]:

$$\hat{H}_{\mathrm{m}} = \sum_i |i\rangle H_{\mathrm{m}}^{(i)}(\mathbf{q})\langle i|, \quad (3)$$

where $\mathbf{q} \equiv \{\hat{\mathbf{R}}_l\}$ denotes the complete set of nuclear coordinates and $|i\rangle$ is the adiabatic electronic state. The adiabatic eigenstates depend on the nuclear coordinates and $H_{\mathrm{m}}^{(i)}(\mathbf{q})$ is the nuclear Hamiltonian for the ith electronic state

$$H_{\mathrm{m}}^{(i)}(\mathbf{q}) = T(\mathbf{q}) + \Omega_i(\mathbf{q}), \quad (4)$$

where $T(\mathbf{q})$ is the nuclear kinetic energy and $\Omega_i(\mathbf{q})$ is the adiabatic potential of the state of $|i\rangle$. Expanding the $\mathrm{Tr}[\cdots]$ in Eq. (2) in the electronic basis, we obtain

$$W_{\mathrm{PP}}^{l} = \frac{1}{2}\frac{1}{\Omega^2\omega}\Re\int \mathrm{d}t \int \mathrm{d}t_3 E_2^*(t)E_2(t-t_3)\exp[\mathrm{i}\omega t_3] \times \sum_{f,g',g''} \mathrm{Tr}_{\mathbf{q}}\Big[\langle g''|\hat{j}_l^{\dagger}(t)|f\rangle\langle f|\hat{j}_l(t-t_3) \times |g'\rangle\langle g'|\tilde{\rho}^{(2)}(t-t_3)|g''\rangle\Big]. \quad (5)$$

Since in NiTPP(Pip)$_2$ the intersystem crossing from T^* to S^* and the subsequent dissociation to S^0 occur in less than a few hundred picoseconds [7], and we focus on the relaxation dynamics from the S^0 state, we can replace the density operator with

$$\tilde{\rho}^{(2)}(t-t_3) \simeq \sum_i |i\rangle\langle i|\rho^{(i)}, \quad (6)$$

where $\rho^{(i)}$ represents the thermal equilibrium in the $|i\rangle$ electronic state. In Eq. (6), we have neglected the off-diagonal elements of the density operator because the dephasing time is much shorter than the detection period. Three electronic states $|i\rangle$ are considered in Eq. (6): The S^0 state with square planar geometry, $|i\rangle = |\mathrm{ES}\rangle$, the transient electronic state with the pyramidal configuration NiTPP(Pip), $|i\rangle = |\mathrm{TS}\rangle$ (see [11, Fig. 1]), and the ground state of NiTPP(Pip)$_2$ with octahedral geometry, $|i\rangle = |\mathrm{GS}\rangle$. The density matrix then reads

$$\tilde{\rho}^{(2)} \simeq |\mathrm{ES}\rangle\langle\mathrm{ES}|\rho^{\mathrm{ES}} + |\mathrm{TS}\rangle\langle\mathrm{TS}|\rho^{\mathrm{TS}} + |\mathrm{GS}\rangle\langle\mathrm{GS}|\rho^{\mathrm{GS}}. \quad (7)$$

Substituting Eq. (7) into Eq. (5) we then have

$$W_{\mathrm{PP}}^{l} = \frac{1}{2}\frac{1}{\Omega^2\omega}\Re\sum_{i=\mathrm{ES,TS,GS}}\int \mathrm{d}t \int \mathrm{d}t_3 E_2^*(t)E_2(t-t_3) \times \exp[\mathrm{i}\omega t_3]\sum_f \mathrm{Tr}_{\mathbf{q}}\left[\left|\langle i|\hat{j}_l|f\rangle\right|^2\rho^i\right]. \quad (8)$$

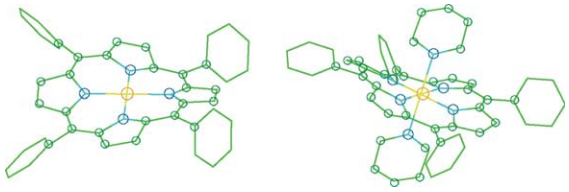

Fig. 1. X-ray geometries of the NiTPP and NiTPP(Pip)$_2$ molecules. Atoms used in the XANES simulations are circled. Green = C, blue = N, Yellow = Ni.

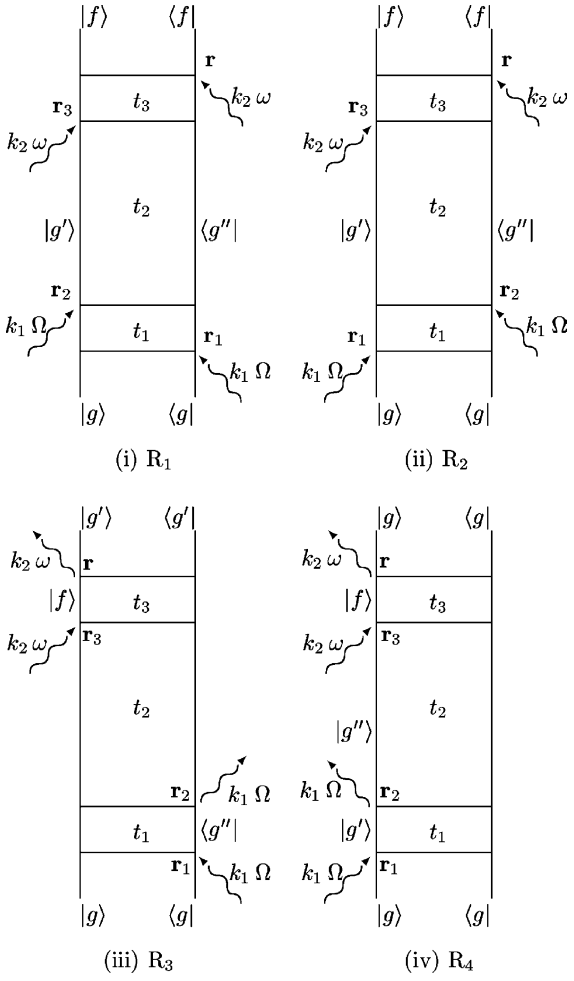

Fig. 2. Liouville space pathways for pump–probe spectroscopy.

Since the core hole lifetime due to the Auger decay is less than 0.5 fs which is far shorter than the X-ray pulse duration of 100 ps, we can assume that the envelope of $E_2(t)$ is constant in the integrand. This gives

$$W_{\mathrm{PP}} \propto \sum_{i=\mathrm{ES,TS,GS}} \mu^i(\omega), \tag{9}$$

where $\mu^i(\omega)$ are the X-ray absorption spectrum components associated with the ES, TS, and GS states:

$$\mu^i(\omega) \equiv \sum_f \mathrm{Tr}_{\mathbf{q}}\left[\rho^i |\langle i|\hat{V}|f\rangle|^2\right] L(\omega_f - \omega_i - \omega). \tag{10}$$

$L(\cdots)$ is a Lorentzian function with the lifetime broadening (FWHM) $\Gamma = 1.58$ eV and $\hat{V}$ denotes the atomic dipole transition operator for Ni 1s core orbital. A complete account of this "Golden Rule" which forms the basis of the traditional multiple scattering X-ray absorption theory is given in the review by Rehr and Albers [12]. This is described briefly below.

We have calculated the X-ray absorption spectrum component with respect to the ES, TS, and GS states, respectively. Using the one electron Green's function

$$G(E) = (E - H + \mathrm{i}\Gamma)^{-1} = \sum_f \frac{|f\rangle\langle f|}{E - E_f + \mathrm{i}\Gamma}, \tag{11}$$

where H is the Hamiltonian, we can rewrite Eq. (10) as

$$\mu^{(i)}(\omega) = 4\pi^2 \mathrm{Im}\langle i|\hat{V}G(\omega)\hat{V}|i\rangle(1 - F(\omega)), \tag{12}$$

where $F(\omega)$ is the occupied fraction of states at energy ω. For a system in thermal equilibrium at room temperature, we can approximate $1 - F(\omega) = \theta(\omega - \mu_F)$, where μ_F is the chemical potential, giving

$$\mu^{(i)}(\omega) = 4\pi^2 \mathrm{Im}\langle i|\hat{V}G(\omega)\hat{V}|i\rangle\theta(\omega - \mu_F). \tag{13}$$

The multiple scattering method is based on the one electron Green's function $G(E)$ for the molecule, solid, or cluster of interest. The Green's function can be represented in an operator form as

$$G = G_0(1 - tG_0)^{-1} \tag{14}$$

where G_0 is the free atom Green's function and $t = v_0 + v_0 G_0 t$ with v_0 the potential seen by the electron described by the Green's function. These operators are represented as complex, non-sparse matrices in a vector space spanned by the basis of local scattering states labeled by angular momenta and atomic coordinates $|L, R_j\rangle = |l, m, R_j\rangle$. In this basis, the free atom Green's function is given by the Rehr–Albers separable representation [13].

The atomic potentials are approximated as spherically symmetric muffin–tin potentials. In this approximation, the t operator is diagonal in the angular momentum site basis $t_{Lj,L'j'}(E) = \exp(\mathrm{i}\delta_{l,j}(E))\sin(\delta_{l,j}(E))\delta_{L,L'}\delta_{j,j'}$ where $\delta_{l,j}(E)$ is the electron scattering phase shift for angular momentum l and site j. Calculating these phase shifts requires the scattering potential for an electron with energy E. This is given by the sum of the coulomb potential and an energy-dependent self-energy. The ground state self-energy is taken as the von Barth–Hedin exchange correlation potential [14] with an energy dependent correction given by the Hedin–Lundqvist self-energy [15]. The charge distribution can be initially taken as that of the free atom. Once the Green's function in the angular momentum site representation is found, $G(\mathbf{r}, \mathbf{r}', E)$ can be calculated [16], and the electron density extracted from this Green's function

$$\rho(\mathbf{r}) = -\frac{2}{\pi}\mathrm{Im}\int_{-\infty}^{\mu_F} \mathrm{d}E\, G(\mathbf{r}, \mathbf{r}, E). \tag{15}$$

This allows the electron density and the Green's function to be solved iteratively and self-consistently.

3. Numerical simulations

The present simulation was carried out using the software package FEFF 8.2 [16]. This code uses the real space multiple scattering Green's function technique described above to simulate XAS, including the extended X-ray absorption fine structure (EXAFS) and XANES. Due to the local nature of XAS, extended systems can be modeled as a relatively small cluster (a few dozen to a few hundred atoms) around the absorbing site. Thus, it can handle simulations of crystals [17], disordered solids [18], liquids, solvated systems [19], and clusters [20]. Molecules [21] can be modeled by specifying the real space coordinates of the atoms; for large molecules, atoms distant from the absorbing site can be neglected. The code explicitly includes all electrons (i.e., does not use pseudopotentials), is relativistic, and can handle all elements up to atomic number 100 (Fermium).

FEFF employs a quasiparticle procedure which ignores many-body excitations. These can be added phenomenologically as an amplitude reduction, but these excitations are weak when the photoelectron energy is small compared to the plasma frequency of the material [22] due to the mutual screening of the photoelectron and the core hole. Similarly, thermal effects cannot be correctly accounted for by Eq. (14) without performing a computationally expensive average over configurations of a thermal ensemble. These effects, however, are small for low energies above the absorption threshold, and are typically only significant in the EXAFS region. As a result, both many-body and thermal effects are neglected in the present calculations.

The structure of NiTPP and NiTPP(Pip)$_2$ was taken from X-ray crystallography data [23,24]. In both cases, the XANES spectra were calculated for a single porphyrin molecule. The nickel was placed at the origin, and the nitrogens along the Cartesian axes. The carbon first and second neighbors of the nitrogens were used,

including the ruffling of the porphyrin molecule. Since XAS is a local probe of the environment of the absorbing atom [12], atoms farther than a few nearest-neighbors are unlikely to have a significant effect. Consequently, farther carbon atoms, including the phenyl rings, were neglected. Thus a total of 29 atoms for NiTPP and 41 atoms for NiTPP(Pip)$_2$ were needed (as indicated by circles in Fig. 1). The coordinates of these atoms were then used as input for the FEFF code version 8.2 [16] to generate the Ni K-edge XANES spectrum.

A cluster of all atoms out to 4.6 Å was used to find the ground state atomic potentials in FEFF's self-consistent potential calculation. While the normal practice for this part of the calculation is to approximate all atoms of the same atomic number Z to have identical potentials, we allowed for the possibility that the environments of the piperidine nitrogens may be sufficiently different from the porphyrin nitrogens to have notably different potentials. However, the only effect of considering these two potentials separately was a red shifting of the XANES by 0.4 eV. All atoms out to 5.0 Angstroms were used in the matrix inversion of Eq. (14) to find the XANES.

Using the X-ray diffraction geometry of the NiTPP(Pip)$_2$ molecule, the XANES signatures of the ligands were investigated by selectively removing one or both ligands and repeating the calculation, keeping the rest of the molecular geometry intact. This allows the separation of the ligand effects from the accompanying changes in the Ni–N bond length on the XANES.

The measured XANES for the nickel porphyrins were not obtained from crystals; NiTPP(Pip)$_2$ was in piperidine solution while NiTPP was measured in toluene. To better compare with experiment, additional FEFF calculations were carried out using crystal atomic coordinates modified by EXAFS Ni–N bond length measurements for the molecule in solution. The X-ray crystal structure was represented as a Z-matrix with all Ni–N distances included as parameters. For both NiTPP and NiTPP(Pip)$_2$ these Ni–N distances were then set to the values measured by Chen et al. [4].

4. Results

In NiTPP(Pip)$_2$, the nickel is octahedrally coordinated with nitrogen atoms. From the X-ray crystallography data, the nitrogens in the porphyrin plane are located 2.04 Å from the nickel, while the piperidine nitrogens are found at an increased distance of 2.26 Å [23]. In this configuration, all 4P orbitals of the nickel hybridize with a 2P orbital from each nitrogen that the orbital is pointing toward. The resulting σ bonding orbitals are all filled with the electrons donated by the nitrogens, while the σ^* orbitals form the lowest lying unoccupied states with P symmetry. The spectral component μ^{GS} is shown in Fig. 3 (black line). The main near-edge transition upon absorption of an X-ray is thus $1S \rightarrow \sigma^*$, which consists of a three-peak-structure in the 8345 to 8365 eV region, as shown in Fig. 3. Since the bond lengths between the nickel and the piperidine nitrogens are longer than those with the porphyrin nitrogen, the σ^* states are split into σ_z^* and $\sigma_{x,y}^*$ states because of the difference of the hybridizations for in-plane and out-of-plane, i.e., *crystal field splitting*. The 8347 eV peak is, therefore, attributed to the transition to the σ_z^* state and the rest are due to those to the $\sigma_{x,y}^*$ states.

With the axial piperidine ligands removed, the nickel is coordinated with nitrogens in a square planar geometry, which is the structure of the S^0 (ES) state. The porphyrin contracts around the nickel, with the nitrogen–nickel bond distance shrinking to 1.93 Å [24]. The $4P_{x,y}$ orbitals of the nickel hybridize with the 2P orbitals from the nitrogen as before, to give $\sigma_{x,y}$ and $\sigma_{x,y}^*$ molecular orbitals. The $4P_z$ orbital, however, is localized because there is no axial ligand molecular orbitals which can hybridize with the nickel $4P_z$ state. The spectral component of μ^{ES} is shown for two geometries in Fig. 3, the blue line shows the spectrum for the fully relaxed geometry of the crystal, where the green line shows the spectra where the porphyrin geometry is unchanged from that of NiTPP(Pip)$_2$ and only the axial piperidines are removed. In both geometries, the lowest energy peak at 8337 eV is attributed to the transition to the localized nickel $4P_z$ state, while the σ_z^* disappears. We can thus confidently attribute this change to the ligands alone. Meanwhile, when the molecule is allowed to relax, the peaks between 8348 and 8360 eV undergo a blue shift of

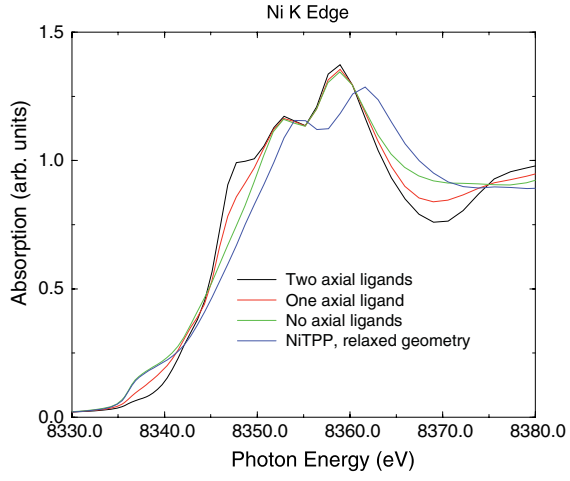

Fig. 3. The effect of the removal of one or both piperidine ligands from the NiTPP(Pip)$_2$ is shown. The reduction of the 8347 eV peak with decreasing piperidines is evident, as is the growth of the shoulder at 8340 eV. When the NiTPP without piperidine ligands is allowed to relax to its equilibrium state, a blue shifting of the structure between 8347 and 8360 eV of about 3 eV is observed.

2–4 eV. Because of the contraction of the bond length between the nickel and the porphyrin nitrogens, the hybridization between the nickel $4P_{x,y}$ and the porphyrin nitrogen 2P orbitals becomes stronger, resulting in the $\sigma^*_{x,y}$ states occurring at a higher energy than in NiTPP(Pip)$_2$ case.

The red line in Fig. 3 shows the spectral component of μ^{TS} in which the pyramidal geometry is assumed and the bond lengths are taken to be equal to those of NiTPP(Pip)$_2$. While the spectrum is coincident with that of NiTPP(Pip)$_2$ (black line) for the $\sigma^*_{x,y}$ states from 8348 eV to 8362 eV, the spectra in the lower energy region differ. In this case, since there is only one axial piperidine ligand, the hybridization of nickel $4P_z$ and the piperidine nitrogen $2P_z$ becomes weak, and one would expect a weakly hybridized orbital to be situated intermediate in energy to the $4P_z$ in NiTPP and the σ^*_z in NiTPP(Pip)$_2$. Our calculations do not show this, instead we see two weak peaks, corresponding to the $4p_z$ transition of NiTPP, and to the σ^*_z transition of NiTPP(Pip)$_2$.

In Fig. 4 we compare the pump–probe difference spectra of NiTPP(Pip)$_2$, NiTPP(Pip), and NiTPP in the unrelaxed geometry around the low energy region of the XANES peak. We note that as the piperidine ligands are removed, the $4P_z$ transition at 8337 eV increases while the σ^*_z transition at 8347 eV decreases in intensity.

Due to the neglect of non-spherical contributions to the potentials, the FEFF 8.2 code often has difficulties reproducing the details of transitions to bound states. In order to compare directly to the measured spectra in solution, the spectral components of μ^{ES} and μ^{GS} are shown in Fig. 5 for the case where the Ni–N bond distances are set to the EXAFS measured values in solution. The experimental results are shown as well. The primary difference is that the σ^*_z peak coincides with the $\sigma^*_{x,y}$ peak, due to the identical Ni–N bond lengths in

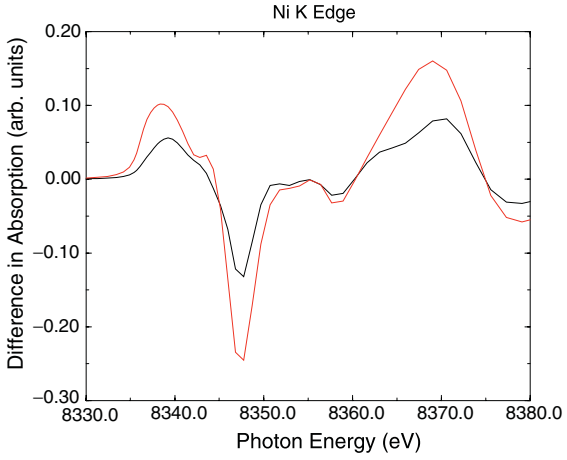

Fig. 4. The difference in the XANES of NiTPP(Pip)$_2$ as one (black) or both (red) piperidines are removed, relative to the XANES of NiTPP(Pip)$_2$ with all of its ligands. This emphasizes the growth of the 8340 eV peak and the reduction of intensity at 8347 eV.

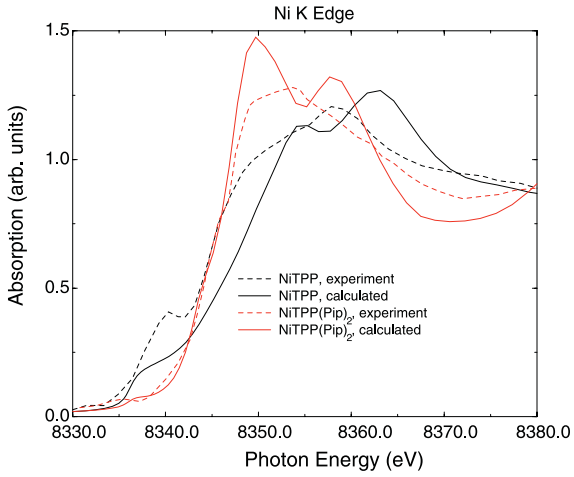

Fig. 5. X ray absorption comparison of the calculations (solid) with the measurements by Chen et al. (dashed). Red curves represent NiTPP(Pip)$_2$, black curves are NiTPP.

both the porphyrin ring and the piperidine ligands. The calculated values show a larger line splitting of the $\sigma^*_{x,y}$ peaks as compared to experiment. In NiTPP, the lower energy side of the σ^* peaks are weaker than in the experiment, as is the lowest peak at 8337 eV. The latter may be due to the core exciton effect, or many-body effect, which are not fully taken into account in the present calculation. However, the main experimental trends are reproduced in the computations; the appearance of a small peak at 8337 eV, the reduction of the peak intensity near 8350 eV, and the blue shift of the near-edge structure beyond 8350 eV.

5. Discussion

Recent advances in the generation of ultrashort X-ray pulses [25–27] have made it possible to use X-rays to examine photoexcited chemical states. In particular, the X-ray absorption spectrum can reveal details about the electronic state of the system and the geometry of the atoms in the vicinity of the X-ray absorbing species. Several optical-pump, X-ray-probe experiments have already been carried out on molecular systems including ruthenium (II) Tris-2,2′-bipyridine $[Ru(bpy)_3]^{2+}$ [28], iodine photodetachment in water [29], and diplatinum tetrapyrophosphate $[Pt_2(pop)_4]^{4-}$ [30]. The recent investigation of the production of a transient population of NiTPP from NiTPP(Pip)$_2$ by Chen et al. [4] which is the focus of this study is based is a typical example of such experiments.

The present study demonstrates the utility of electronic structure simulations for the interpretation of X-ray absorption spectra: XANES spectra may be calculated for any fixed molecular geometry. If an X-ray pulse is shorter than the vibrational period in a molecule,

we can detect the change of the electronic structure and the local structural change around the target atom with time-resolved X-ray absorption, just like our recent simulation of time-resolved X-ray diffraction of polydiacetylene [31].

The observed spectra are given by the averaged sum of the spectral components of the various species as shown in Eq. (9). Since we have calculated each spectral component $\mu^i(\omega)$, we can in principle extract the relative ratio of the state population ρ^i by comparison with experiment. This information is crucial in clarifying the relaxation dynamics after optical-pulse excitation.

The ability of the FEFF code to reproduce many of the observed experimental features is a promising start. Software tools like FEFF have been developed for investigating the ground state X-ray absorption. However, an optical pump leaves the system in an excited electronic state. While this has no effect on the measurement of geometry changes with EXAFS, the near-edge spectrum depends sensitively on the electronic state of the system [12]. This complicates the modeling of near-edge X-ray absorption of optically excited molecules. Clearly, for more general applicability, the XAS codes must be extended to handle excited electronic states. By modifying FEFF's atomic potentials off which the photoelectron can scatter based on the electron density of the photoexcited state, the density of states of the excited chemical species could be calculated. This can be done, for example, by specifying within the FEFF program the electron occupation of the atomic orbitals of each atom in the molecule that undergoes charge transfer, or, alternately, by taking the change in the electron distribution from time dependent ab initio (e.g., density functional) electronic structure calculations. This approach should yield the density of states of the molecule in its excited electronic state, allowing a first principle prediction of XANES.

The time-resolved X-ray absorption in the soft-X-ray region may be a powerful probe of the change of the transition metal 3d electronic states by optical-pump excitation. It is well known that many transition metal $2p \rightarrow 3d$ soft-X-ray absorption spectra have a rich structure due to strong multiplet interactions between the 2p core hole and 3d electrons as well as charge transfer effects [32]. Time-resolved nickel $2p \rightarrow 3d$ X-ray absorption spectroscopy can reveal in detail the relaxation dynamics of the 3d spin state from the singlet S^0 to triplet T^0 states, where the one electron promotion from $3d_{Z^2}$ and $3d_{X^2-Y^2}$ occurs.

Other signatures of an excited state in the time-resolved X-ray absorption include satellites preceding the main absorption edge. These satellites show up when the absorbing core electron is promoted to the valence hole of the optically excited state or because of a shake-down process where the excited valence electron or valence hole undergo transitions to lower energy states.

The approach described in this paper holds promise for interfacing with molecular dynamics simulations. Given a time series of snapshots from the molecular dynamics, the coordinates could be input into an XAS code such as FEFF. The evolution of the XANES could then be followed in real time as the molecular geometry changes.

Acknowledgements

The authors would like to thank Dr. Lin Chen for most useful discussions. This work was supported by the Laboratory Directed Research and Development Program of Lawrence Berkeley National Laboratory under the Department of Energy Contract No. DE-AC03-76SF00098. The support of the Chemical Sciences Division, Office of Basic Energy Sciences, US Department of Energy Grant DE-FG02-01ER15155 is gratefully acknowledged.

References

[1] M. Hentschel, R. Kienberger, Ch. Spielmann, G.A. Reider, N. Milsevic, T. Brabec, P. Corkum, U. Heinzmann, M. Drescher, F. Krausz, Nature 414 (2001) 509.
[2] F.L.H. Brown, K.R. Wilson, J. Cao, J. Chem. Phys. 111 (1999) 6238.
[3] P.M. Rentzepis, J. Helliwell, Time-Resolved Electron and X-ray Diffraction, Oxford Press, New York, 1995.
[4] L.X. Chen, W.J.H. Jäger, G. Jennings, D.J. Gosztola, A. Munkholm, J.P. Hessler, Science 292 (2001) 262.
[5] D. Kim, C. Kirmaier, D. Holten, Chem. Phys. 75 (1983) 305.
[6] D. Kim, D. Holten, Chem. Phys. Lett. 98 (1983) 584.
[7] J. Rodriguez, D. Holten, J. Chem. Phys. 92 (1990) 5944.
[8] H.S. Eom, S.C. Jeoung, D. Kim, J.-H. Ha, Y.-R. Kim, J. Phys. Chem. A 101 (1997) 3661.
[9] S. Tanaka, V. Chernyak, S. Mukamel, Phys. Rev. A 63 (2001) 63405.
[10] S. Mukamel, Principles of Nonlinear Optical Spectroscopy, Oxford, New York, 1995.
[11] L.X. Chen, J. Electron. Spectrosc. Relat. Phenom. 119 (2001) 161.
[12] J.J. Rehr, R.C. Albers, Rev. Mod. Phys 72 (2000) 621.
[13] J.J. Rehr, R.C. Albers, Phys. Rev. B 41 (1990) 8139.
[14] U. von Barth, L. Hedin, J. Phys. C 5 (1972) 1629.
[15] B.I. Lundqvist, Phys. Condens. Mater. 6 (1967) 193.
[16] A.L. Ankudinov, B. Ravel, J.J. Rehr, S.D. Conradson, Phys. Rev. B 58 (1998) 7565.
[17] H. Modrow, S. Bucher, J.J. Rehr, A.L. Ankudinov, Phys. Rev. B 67 (2003) 035125.
[18] A. Garcìa-Arribas, M.L. Fdez-Gubieda, J.J. Rehr, J. Non-Crystal. Solids 287 (2001) 60.
[19] L. Campbell, J.J. Rehr, G.K. Schenter, M.I. McCarthy, D. Dixon, J. Synchrot. Radiat. 6 (1999) 310.
[20] A.L. Ankudinov, J.J. Rehr, Phys. Rev. Lett. 86 (2001) 1642.
[21] N. Haack, G. Ceballos, H. Wende, K. Baberschke, D. Arvanitis, A.L. Ankudinov, J.J. Rehr, Phys. Rev. Lett. 84 (2000) 614.
[22] L. Campbell, L. Hedin, J.J. Rehr, W. Bardyszewski, Phys. Rev. B 65 (2001) 064107.
[23] S.-L. Jia, W. Jentzen, M. Shang, X.-Z. Song, J.-G. Ma, W.R. Scheidt, J.A. Shelnutt, Inorg. Chem. 37 (1998) 4402.

[24] A.L. Maclean, G.J. Foran, B.J. Kennedy, P. Turner, T.W. Hambley, Aust. J. Chem. 49 (1996) 1273.
[25] R.W. Schoenlein, W.P. Leemans, A.H. Chin, P. Volfbeyn, T.E. Glover, P. Balling, M. Zolotorev, K.-J. Kim, S. Chattopadhyay, C.V. Shank, Science 274 (1996) 236.
[26] R.W. Schoenlein, S. Chattopadhyay, H.H.W. Chong, T.E. Glover, P.A. Heimann, C.V. Shank, A.A. Zholents, M.S. Zolotorev, Science 287 (2000) 2237.
[27] A. Rousse, P. Audebert, J.P. Geindre, F. Falliès, J.C. Gauthier, Phys. Rev. E 50 (1994) 2200.
[28] M. Saes, C. Bressler, R. Abela, D. Grolimund, S.L. Johnson, P.A. Heimann, M. Chergui, Phys. Rev. Lett. 90 (2003) 047403.
[29] C. Bressler, M. Saes, M. Chergui, D. Grolimund, R. Abela, P. Pattison, J. Chem. Phys. 116 (2002) 2955.
[30] C.D. Kim, S. Pillet, G. Wu, W.K. Fullagar, P. Coppens, Acta Crystallogr. A 58 (2002) 133.
[31] S. Tanaka, S. Volkov, S. Mukamel, J. Chem. Phys 118 (2003) 3065.
[32] J. Fink et al., Phys. Rev. B 32 (1985) 4889.